DOI: 10.24850/j-tyca-2021-04-03

Articles

Hydraulic analysis of a compound weir (triangular-rectangular) simulated with computational fluid dynamics (CFD)

Análisis hidráulico de un vertedor compuesto (triangular-rectangular) mediante dinámica de fluidos computacional (CFD)

Erick Dante Mattos-Villarroel[1], ORCID: https://orcid.org/0000-0002-5640-5213

Jorge Flores-Velazquez[2], ORCID: https://orcid.org/0000-0003-0895-4645

Waldo Ojeda-Bustamante[3], ORCID: https://orcid.org/0000-0001-7183-9637

Mauro Iñiguez-Covarrubias[4]

Carlos Díaz-Delgado[5], ORCID: https://orcid.org/0000-0001-6245-070X

Humberto Salinas-Tapia[6], ORCID: https://orcid.org/0000-0002-0075-6997

[1]Instituto Mexicano de Tecnología del Agua, Jiutepec, Morelos, Mexico, e_mattos_@outlook.com

[2]Instituto Mexicano de Tecnología del Agua, Jiutepec, Morelos, Mexico, jorgelv@colpos.mx

[3]Colegio Mexicano de Ingenieros en Irrigación, Morelos, Mexico, w.ojeda@riego.mx

[4]Instituto Mexicano de Tecnología del Agua, Jiutepec, Morelos, Mexico, mic@tlaloc.imta.mx

[5]Instituto Interamericano de Tecnología y Ciencias del Agua, Universidad Autónoma del Estado de México, Toluca, State of Mexico, Mexico, cdiazd@uaemex.mx

[6]Instituto Interamericano de Tecnología y Ciencias del Agua, Universidad Autónoma del Estado de México, Toluca, State of Mexico, Mexico, hsalinast@uaemex.mx

Correspondence author: Jorge Flores-Velazquez, jorgelv@colpos.mx

Abstract

To make an efficient delivery of water to irrigation users, it is necessary to have accurate dispositive to measure flow rates. These dispositive include triangular and rectangular weirs for measured flow rates ranges between 30 and 200 l s^{-1}. However, the variation of flows in the execution of an agricultural year can be a factor of error in the volumetric delivery and a possible alternative solution is the use of a compound weir. The aim of this study was to analyze the hydraulic behavior of a triangular-rectangular weir, as a function of geometric and flow parameters and get

a new global expression of the discharge coefficient. ANSYS Fluent was used to simulate the flow rates fluid, to discretized the dynamics of flow under specific conditions. The evaluation of the model with ANSYS Fluent, and its analysis, was carried out based on experimental data and the corresponding analytical solution. The Computational Fluid Dynamics (CFD) simulations showed statistical agreement with the laboratory data, finding a maximum error of 0.74 %. An expression of the global discharge coefficient was obtained and it was possible to analytically estimate the expenditure with a maximum error of 7.8 % with respect to experimental data. Thanks to the CFD simulation, it was possible to characterize the nappe and to analyze the effects of pressure and velocity on the discharge coefficient. The results allow us to conclude that a triangular-rectangular weir widely satisfies the precision required in the delivery of water to irrigation users.

Keywords: Weir, numerical simulation, gauging, discharge coefficient.

Resumen

Para hacer una entrega eficiente de agua a usuarios de riego es necesario contar con dispositivos precisos para medir gastos. Entre estos dispositivos están los vertedores triangulares y rectangulares para rangos de flujo entre 30 y 200 l s^{-1}. Sin embargo, la variación de gastos en un año agrícola puede ser un factor de error en la entrega volumétrica, y una posible alternativa de solución es el uso de un vertedor compuesto. El objetivo de este trabajo fue analizar el comportamiento hidráulico de un vertedor triangular-rectangular en función de sus parámetros

geométricos y de flujo, así como obtener una expresión de su coeficiente global de descarga. *ANSYS Fluent* fue usado para simular los caudales del fluido, con el fin de discretizar la dinámica del flujo bajo condiciones específicas. La evaluación del modelo con ANSYS Fluent, y su análisis, fue efectuada con base en datos experimentales y la solución analítica correspondiente. Las simulaciones con la dinámica de fluidos computacional (CFD) mostraron concordancia estadística con los datos de laboratorio, encontrándose un error máximo de 0.74 %. Se obtuvo una expresión del coeficiente global de descarga y se logró estimar analíticamente el gasto con un error máximo de 7.8 % con respecto a datos experimentales. Gracias a la simulación con CFD fue posible caracterizar la lámina de descarga y analizar los efectos de la presión y la velocidad sobre el coeficiente de descarga. Los resultados permiten concluir que un vertedor triangular-rectangular satisface ampliamente la precisión requerida en la entrega de agua a usuarios de riego.

Palabras clave: vertedor, simulación numérica, aforo, coeficiente de descarga.

Received: 09/01/2020

Accepted: 27/02/2020

Introduction

The effect on the conservational and efficient use of water resources now has an impact on improving water management. One of the components of integrated water resources management (IWRM) is the ability to accurately measure and control water flow at specific points in a basin or in a distribution system, such as: Channel bifurcations, control structures, and water delivery points. An efficient water measuring system allows accurate accounting of water use, and the supply of water at optimal rates to areas of demand (Clemmens, Wahl, Bos, & Replogle, 2001). Several types of structures can be used for flow gauging: weirs, Parshall gauges, gates, orifices, among others (Skertchly, 1988).

Weirs are elevated barriers located perpendicular to the direction of water movement so that water rises above the obstruction through an opening on a regular basis (Bautista, Robles, Júnez, & Playán, 2013). The geometric parameters defining the hydraulic behavior of weirs are the length of the ridge and the shape of the flow control section (Emiroglu, Kaya, & Agaccioglu, 2010; USBR, 1997). Thin-walled weirs are studied using the principles of classical physics with experimental results to understand flow characteristics and determine the coefficient of discharge (C_d) under different configurations; this coefficient integrates the effects not considered in the derivation of equations used to estimate discharge, such as viscosity, capillarity, surface tension, velocity distribution and aerodynamic curvature attributable to weir contraction (Aydin, Altan-Sakarya, & Sisman, 2011; Rady, 2011).

Design Specifications and proper installation of weirs have been documented by the British Standards Institute (BSI, 1965), the International Standardization Organization (ISO, 1980), the American Society for Testing Materials (ASTM, 1993), and the United States Bureau of Reclamation (USBR, 1997). Normally, the measurement accuracy of the flow rate depends of the geometry of the weir; in areas with unevenness, triangular weirs are recommended for flow rates lower than 30 l s^{-1} for its greater precision for small discharges, and for higher flow rates rectangular weirs are used (Sotelo, 1997).

Shen (1981) described the procedure for designing sharp-crest triangular weirs supported by experimental results to determine the coefficient of discharge reported in the literature. El-Alfy (2005) experimentally evaluated the effect of the vertical flow curvature on the coefficient of discharge (C_d), in triangular weirs, indicating that it is inversely proportional to the angle of the weir notch (θ) and directly proportional to the relative load (h/P). Bagheri and Heidarpour (2009) obtained a discharge coefficient equation for thin-walled rectangular weirs at the top and bottom of the sheet profiles using the free vortex theory. Bautista *et al*. (2013) used a low-speed photographic technique to characterize the upper and lower profiles of the flow draft on a triangular weir. Chen, Fu, Chen, and Cui (2018) analyzed the effects on the discharge coefficient by the variation of the slope of the ramps implemented on the upstream and downstream faces in a rectangular short-crest weir. Fu, Cui, Dai, and Chen (2018) proposed an equation to determine the discharge coefficient in structures of the orifice-weir type. Tian, Wang, Bai, and Li (2018) investigated the flow pattern and discharge

coefficient at finite crest length combined with parallel walls with the flared entry (FGPs) on the crest of the weir.

It has been reported that the use of compound weirs combining triangular and rectangular shapes for flow measurement gives good results (Zahiri, Tang, & Azamathulla, 2014). Negm, Al-Brahim, and Alhamid (2002) proposed a structure composed of an upper rectangular weir with a lower gate to avoid the accumulation of sediments upstream of the structure. Another type of compound weir consists of a rectangular notch with a triangular notch in the center of the rectangular crest; the triangular weir could accurately measure the normal range of flows less than 30 l s^{-1}, but larger flows can also be measured by operating the rectangular weir (USBR, 1997). In irrigation channels with the variability of discharge, the use of compound weirs is recommended to avoid the use of separate structures, which can represent the variability of flow with greater precision; to meet this need, weir structures described in this document play a key role in irrigation zones.

Numerical simulation techniques have been used to solve Fluid Mechanics problems, particularly with the use of general solution tools generically called Computational Fluid Dynamics (CFD). Advances in computer storage and processing capacity allowed the process of creating and fitting a CFD model to evolve and facilitate the analysis of results, both in time and cost. In particular, CFD techniques numerically solve the governing equations of the flow, such as the Navier-Stokes equations, and offer the possibility of hydraulically evaluating a weir under different geometries and hydraulic conditions. In fact, once validated and evaluated, CFD allows the extraction of additional information, such as:

Forces, velocity fields, and pressures. Several studies have shown the advantages of CFD techniques, for example, Ho, Boyes, and Donohoo (2001), and Ho, Boyes, Donohoo, and Cooper (2003) compared numerical results from a Creager crest weir and reported results very similar to experimental studies using physical models. Rady (2011) reported a maximum deviation of ±3 % when comparing the coefficient of discharge of a thin-walled rectangular weir obtained numerically with CFD versus, those calculated with the general weir equation. Zuhair and Zubaidy (2013) compared the CFD results, using the VOF (Volume of Fluid) model, with the experimental data of a prototype of the Mandali weir, the results indicate that the flow profile obtained with CFD adjusts to the experimental results with a Pearson correlation coefficient close to 1. Therefore, the CFD methodology constitutes an effective tool to solve fluid mechanics problems related to hydraulic weirs.

Representation of physics-free surface phenomena, in the experimental or analytical models, represent one of the most difficulties in this area. CFD simulation can be an excellent option in order to investigate modeling on weirs and simulate numerical flow and tracking in detail of the free surface. In analyzing this problem, the use of CFD has been reported, in particular, the computational platform ANSYS-FLUENT, known for its ability to accurately track the free surface using the Volume Of Fluid (VOF) method (Duró, Dios, López, Liscia, & Angulo, 2012).

The aim of this work was (1) to build and evaluate a numerical model of a compound weir using Computational Fluid Dynamics (CFD) and (2) to propose a global discharge coefficient equation for the compound weir (triangular-rectangular). The numerical simulation of compound

weirs will facilitate the understanding of its hydraulic behavior, which depends on the geometric characteristics of the weir, its hydraulics conditions, and the estimated discharge coefficient.

Materials and methods

Reference Prototype model

Experimental data and prototype models used are reported by Sotelo (1997), to using rectangular and triangular weir thin-walled, and Jan, Chang, and Lee (2006) in compound weirs. Figure 1 shows the geometric dimensions of the rectangular and triangular weirs, both weirs are independent in a channel with a hydraulic load of 0.27 m for the rectangular weir, and 0.50 m for the triangular weir. Both weirs are sharp-crest for the operation, and for the simulation standard wall value were used (Skertchly, 1988).

Tecnología y ciencias del agua, ISSN 2007-2422, 12(4), 112-162. DOI: 10.24850/j-tyca-2021-04-03

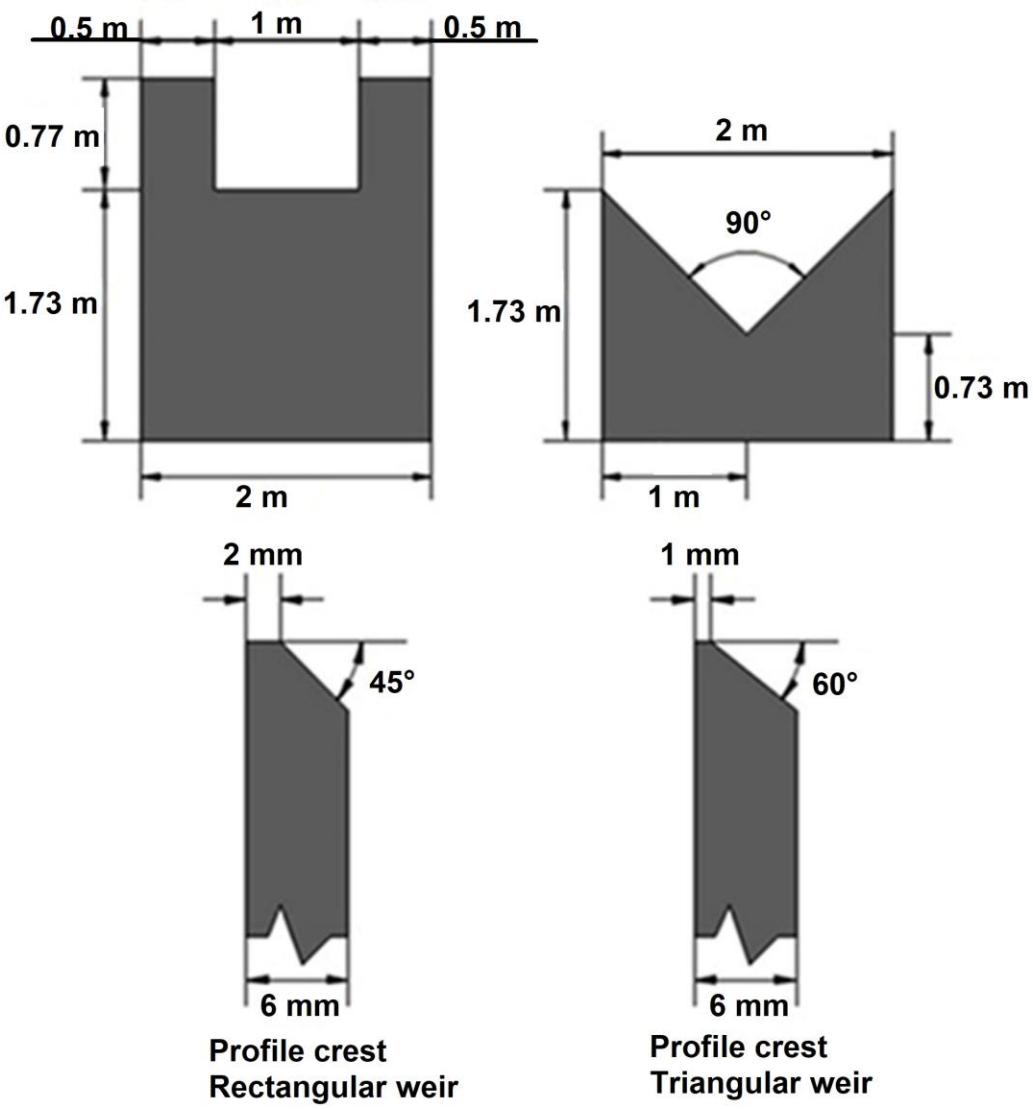

Figure 1. Dimensions of the rectangular and triangular prototypes weirs (Sotelo, 1997; Skertchly, 1988).

Analytic weir equations

Tecnología y ciencias del agua, ISSN 2007-2422, 12(4), 112-162. DOI: 10.24850/j-tyca-2021-04-03

Experimental and analytical studies were performance on the flow behavior upstream and downstream of the weir, for instance, upstream near the weir there is a speed varied movement and present a backwater of depression originating the transformation of potential energy into kinetic energy, there is a zone of stagnation of the water called dead water. Upstream of the weir, there is gradually varied flows; this area is up to a distance of 4*h*, *h* being the static charge on the crest of the weir (Sotelo, 1997).

Equation (1) shows the general form that allows obtaining the fluid flow through a weir (Bos, 1989).

$$Q = k\, h^n \qquad (1)$$

Where Q = flow ($m^3\ s^{-1}$); k = coefficient depending on the dimensions and shape of the weir ($m^{1.5}\ s^{-1}$) for a rectangular weir ($m^{0.5}\ s^{-1}$) for a triangular weir), and n = dimensionless number depending on the shape of the weir; for a rectangular and triangular weir n is equal to 1.5 and 2.5, respectively (Bos, 1989).

For Henderson (1966) the discharge equation for a rectangular weir can be simplified as (Equation (2)):

Tecnología y ciencias del agua, ISSN 2007-2422, 12(4), 112-162. DOI: 10.24850/j-tyca-2021-04-03

$$Q = \frac{2}{3} C_d (2g)^{0.5} b\, h^{1.5} \quad (2)$$

Where C_d is the coefficient of discharge (dimensionless); b, the length of the weir crest (m); g, the acceleration of gravity (m s^{-2}), and h is the static load on the weir crest (m). The coefficient of the discharge depends on the flow characteristics and geometry of the channel and weir (Kumar, Ahmad, & Mansoor, 2011).

The triangular section weirs are recommended for the gauging of flow rates less than 30 l s^{-1} and loads from 6 cm to 60 cm; their precision is better than that of a rectangular weir for small flows. For larger discharges, a rectangular weir is recommended, because the triangular weir is more sensitive to any change in the roughness of the plate and because it requires greater accuracy in the measurement of loads. The flow equation for the triangular weir is Equation (3) (Sotelo, 1997):

$$Q = \frac{8}{15} C_d (2g)^{0.5} \tan \theta/_2\, h^{2.5} \quad (3)$$

Where θ is the angle of the notch of the triangular section (°).

The discharge coefficients are calculated with Equation (4) for the rectangular weir and Equation (5) for the case of a triangular weir whose notch angle, θ, is 90° (Sotelo, 1997).

$$C_d = \left[0.6075 - 0.045 \frac{(B-b)}{B} + \frac{0.0041}{h}\right]\left[1 + 0.55 \left(\frac{b}{B}\right)^2 \left(\frac{h}{h+P}\right)^2\right] \quad (4)$$

Tecnología y ciencias del agua, ISSN 2007-2422, 12(4), 112-162. DOI: 10.24850/j-tyca-2021-04-03

$$C_d = \left(0.5812 + \frac{0.00375}{h}\right)\left\{\left[1 + \left[\frac{h^3}{B(h+P)}\right]^2\right]\right\} \quad (5)$$

Where B is channel width (m); b, the length of the rectangular weir (m); P, the height of the weir (m); h, the static load on the weir (m), and C_d is the coefficient of discharge (dimensionless).

Figure 2 shows the compound weirs with rectangular and triangular sections. The discharge equation can be derived using the linear combination method, according to Jan *et al*. (2006), and is expressed with Equation (6):

$$Q = \frac{8}{15} C_{dt} (2g)^{0.5} \tan \theta/_2 \, (h_2^{2.5} - h_1^{2.5}) + \frac{2}{3} C_{dr} (2g)^{0.5} (2b_1) h_1^{1.5} \quad (6)$$

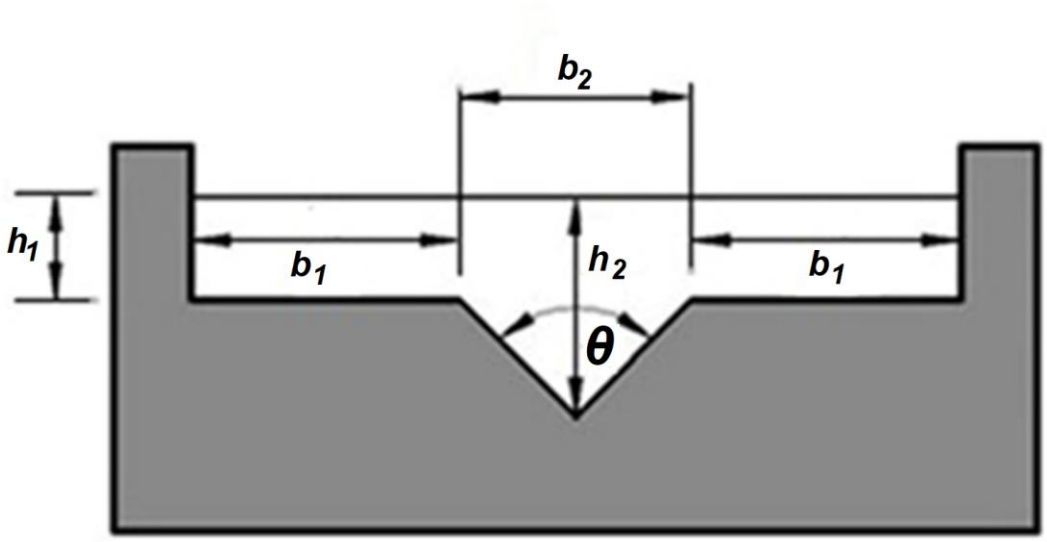

Figure 2. Triangular-rectangular compound weir.

Tecnología y ciencias del agua, ISSN 2007-2422, 12(4), 112-162. DOI: 10.24850/j-tyca-2021-04-03

The compound weir equation (Equation (6)) contains two basic terms: The first one is the discharge of the triangular section $\left[\frac{8}{15}C_{dt}(2g)^{0.5}\tan{}^{\theta}/_{2}\,(h_2^{2.5}-h_1^{2.5})\right]$, and second one corresponding to the discharge of the rectangular section $\left[\frac{2}{3}C_{dr}(2g)^{0.5}(2b_1)h_1^{1.5}\right]$; C_{dt} is the coefficient of discharge of the triangular section (dimensionless); C_{dr} is the coefficient of discharge of the rectangular section (dimensionless); b_1 is the width of the rectangular weir (m); h_1 and h_2 are the static load on the rectangular and triangular section (m), respectively.

The value of C_{dt} can be estimated using the empirical relationship (Jan *et al*., 2006) (Equation (7)):

$$C_{dt} = 0.6085 - 0.0525\theta + 0.02135\theta^2 \qquad (7)$$

The value of C_{dr} depends on load h_1 (m), crest height P (m), length of rectangular section b (m), and width of channel B (m), it is described as Equation (8) (Jan *et al*., 2006):

$$C_{dr} = \frac{0.611+2.23\left(\frac{B}{2b_1}-1\right)^{0.7}}{1+3.8\left(\frac{B}{2b_1}-1\right)^{0.7}} + \frac{0.075+0.011\left(\frac{B}{2b_1}-1\right)^{1.46}}{1+4.8\left(\frac{B}{2b_1}-1\right)^{1.46}}\frac{h_1}{P} \qquad (8)$$

It should be clarified that the C_d values of Equation (4) and Equation (5) are different from C_{dr} and C_{dt} of Equation (7) and Equation (8), the

latter corresponds to a compound weir of rectangular and triangular sections. Sotelo (1997) analyzed just two cases of weirs; the first one using a triangular weir and the second one was a rectangular weir, both with different hydraulics loads, and subsequently evaluated their discharge coefficients based on the level of hydraulics loads obtained in each weir. The results and experimental data are summarized in Table 1.

Table 1. Results and experimental data of the rectangular and triangular weirs were reported by Sotelo (1997).

Weir	Hydraulic load h (m)	Coefficient of discharge C_d	Flow rates Q (l s^{-1})
Rectangular	0.27	0.602	249
Triangular	0.50	0.590	246

On the other hand, for the weir with combined triangular-rectangular section, Jan *et al*. (2006) reported experimental results of discharge for three cases of weirs of different width of the rectangular section (b_1) and different flow rates (Q); Table 2 show the experimental conditions and the results obtained.

Table 2. Experimental conditions and results of the compound weir reported by Jan *et al*. (2006).

Tecnología y ciencias del agua, ISSN 2007-2422, 12(4), 112-162. DOI: 10.24850/j-tyca-2021-04-03

θ (°)	Channel width (m)	b_1 (m)	b_2 (m)	h_1 (m)	h_2 (m)	C_{dr}	C_{dt}	Analytical flow rates Q (l s^{-1})	Experimental flow rates Q (l s^{-1})
90	1.49	0.25	0.20	0.013	0.113	0.590	0.579	7.13	8.06
90	1.49	0.25	0.20	0.031	0.131	0.591	0.579	13.02	14.36
90	1.49	0.25	0.20	0.036	0.136	0.591	0.579	14.95	16.33
90	1.49	0.40	0.20	0.022	0.122	0.594	0.579	11.59	13.35
90	1.49	0.40	0.20	0.041	0.141	0.595	0.579	21.41	23.35
90	1.49	0.40	0.20	0.069	0.169	0.597	0.579	39.90	45.50
90	1.49	0.50	0.20	0.01	0.110	0.595	0.579	7.23	8.06
90	1.49	0.50	0.20	0.023	0.123	0.597	0.579	13.30	14.36
90	1.49	0.50	0.20	0.027	0.127	0.598	0.579	15.53	16.33

Computational Fluid Dynamics (CFD) modeling

ANSYS WORKBENCH V14.5 was used to perform the simulations. CFD is a numerical tool that predicts the behavior of a fluid by solving the general transport equations, also called Navier-Stokes (NS) equations. Because there is no analytical solution, CFD uses the Finite Volume Method (FVM),

Tecnología y ciencias del agua, ISSN 2007-2422, 12(4), 112-162. DOI: 10.24850/j-tyca-2021-04-03

which divides the domain into a finite number of cells over which discrete conservation of the variable is imposed.

General Equations and sub-models

Equation (9) is the differential form of the mass equation balance for incompressible flow (constant density), where $\nabla \cdot \boldsymbol{U}$ represents the velocity variation.

$$\nabla \cdot U = \frac{\partial \mathrm{U_x}}{\partial \mathrm{x}} + \frac{\partial \mathrm{U_y}}{\partial \mathrm{y}} + \frac{\partial \mathrm{U_z}}{\partial \mathrm{z}} = 0 \quad (9)$$

Regarding the incompressible fluid, the momentum differential equation is shown as (Equation (10)):

$$\frac{\partial(\rho \boldsymbol{U})}{\partial t} + \nabla(\rho \boldsymbol{U}\boldsymbol{U}) = \nabla(\mu \nabla \boldsymbol{U}) - \nabla p + \rho f \quad (10)$$

ρ (kg m^{-3}) is the density of the fluid; $\boldsymbol{U}$ (m s^{-1}) is the velocity field; f (N kg^{-1}) are the forces of the body per unit mass; p (N m^{-2}) is dynamic pressure; μ (kg m^{-1} s^{-1}) dynamic viscosity (0.001 kg m^{-1} s^{-1} for 20 °C).

Tecnología y ciencias del agua, ISSN 2007-2422, 12(4), 112-162. DOI: 10.24850/j-tyca-2021-04-03

The Volume of Fluid (VOF) model is a surface tracking technique by defining calculation cells that can be empty, partially filled, or full of fluid. It was reported by Hirt and Nichols (1981) and is based on a concept that the volume occupied by one material cannot be occupied by the other. For each additional phase added to the model, a new variable is introduced: the volume fraction of the phase in the computational cell. In each control volume, the volume fractions of all phases conform the unit. The volume fraction of the fluid q^{th} in the cell is denoted as α_q, then the following three conditions are possible: if $\alpha_q = 0$, the cell is empty of fluid q^{th}; if $\alpha_q = 1$, the cell is full of fluid q^{th}, and if $0 < \alpha_q < 1$, the cell contains the interface between the fluid q^{th} and the rest of the fluids.

The follow-up of the interface between phases is carried out by the solution of the continuity equation (Equation (11), for the volume fraction of one (or more) of the phases. For the q^{th} phase this equation has the following form (Hirt & Nichols, 1981):

$$\frac{1}{\rho_q}\left[\frac{\partial}{\partial t}\left(\alpha_q \rho_q\right) + \nabla \cdot \left(\alpha_q \rho_q v_q\right)\right] = S_{\alpha_q} + \sum_{p=1}^{n}\left(\dot{m}_{pq} - \dot{m}_{qp}\right) \qquad (11)$$

Where ρ_q is the density of the phase q (kg m^{-3}); v_q is the velocity of the phase q (m s^{-1}); S_{α_q} is the term source of the equation (kg m^{-2} s^{-2}); $\dot{m}_{pq}$ the mass transfer from phase p to phase q (kg s^{-1}), and $\dot{m}_{qp}$ the mass transfer from phase q to phase p (kg s^{-1}).

The turbulence model K-ε is a semi-empirical model based on the transport equations for turbulent energy (K) and for the dispersion of

Tecnología y ciencias del agua, ISSN 2007-2422, 12(4), 112-162. DOI: 10.24850/j-tyca-2021-04-03

turbulent kinetic energy (ε) (Launder & Spalding, 1974; Spalart & Almaraz, 1992). In obtaining this model, it is assumed that the turbulent flow is fully developed and that the effects of molecular viscosity are neglected (Jones & Launder, 1972), parameters *K* (m^2 s^{-2}) and ε (m^2 s^{-3}) are obtained from the Equation (12) and Equation (13):

Turbulent kinetic energy (*K*) (Equation (12)):

$$\frac{\partial(\rho K)}{\partial t}+\frac{\partial(\rho U_j K)}{\partial x_j}=\frac{\partial}{\partial x_j}\left[\left(\mu+\frac{\partial \mu_t}{\sigma_k}\right)\frac{\partial K}{\partial x_j}\right]+P_k-\rho\varepsilon+P_{kb} \quad (12)$$

Dispersion of turbulent kinetic energy (ε) (Equation (13)):

$$\frac{\partial(\rho\varepsilon)}{\partial t}+\frac{\partial(\rho U_j \varepsilon)}{\partial x_j}=\frac{\partial}{\partial x_j}\left[\left(\mu+\frac{\partial \mu_t}{\sigma_\varepsilon}\right)\frac{\partial \varepsilon}{\partial x_j}\right]+\frac{\varepsilon}{K}(C_{1\varepsilon}P_k+C_{2\varepsilon}\rho\varepsilon+C_{1\varepsilon}P_{\varepsilon b}) \quad (13)$$

μ_t is the turbulent viscosity (kg m^{-1} s^{-1}) and it is shown as (Equation (14)):

$$\mu_t=\rho C_\mu \frac{K^2}{\varepsilon} \quad (14)$$

P_{kb} and $P_{\varepsilon b}$ represent the influence of floatability force. P_K is the turbulent generation due to the viscous force (kg m^{-1} s^{-3}), as shown below (Equation (15)):

Tecnología y ciencias del agua, ISSN 2007-2422, 12(4), 112-162. DOI: 10.24850/j-tyca-2021-04-03

$$P_K = \mu_t \left(\frac{\partial \mathrm{U}_i}{\partial \mathrm{x}_j} + \frac{\partial \mathrm{U}_j}{\partial \mathrm{x}_i}\right)\frac{\partial \mathrm{U}_i}{\partial \mathrm{x}_j} - \frac{2}{3}\frac{\partial \mathrm{U}_k}{\partial \mathrm{x}_k}\left(\mu_t \frac{\partial \mathrm{U}_k}{\partial \mathrm{x}_{kk}} + \rho K\right) \quad (15)$$

The values of the coefficients C_μ, $C_{1\varepsilon}$, $C_{2\varepsilon}$, σ_k, and σ_ε were adjusted by Launder and Spalding (1974), which are shown as follows: $C_\mu = 0.09$, $C_{1\varepsilon} = 1.44$, $C_{2\varepsilon} = 1.92$, $\sigma_\varepsilon = 1.3$, $\sigma_k = 1.0$.

Numerical CFD simulation

Numerical simulation and solution using CFD consider three basic steps: a) Preprocess, b) Process, and c) Post-process. This a sequential activities, quality, and results depend of each one its activities.

The first step consists of digital generation as a solid of the construction of the physical model under study (Figure 3), to hydraulically analyze weirs in CFD the computational model must be defined as a three-dimensional geometry. The geometry module was used to perform the numerical model. The characteristics of the numerical model are based in a prototype triangular, rectangular, and compound model. Jan *et al*. (2006) and Sotelo (1997) do not mention the slope of the channel on which the tests were carried out; it was assumed that the slope is totally

horizontal and the flow gradually varied so that the discharge coefficient is not affected by the slope of the channel.

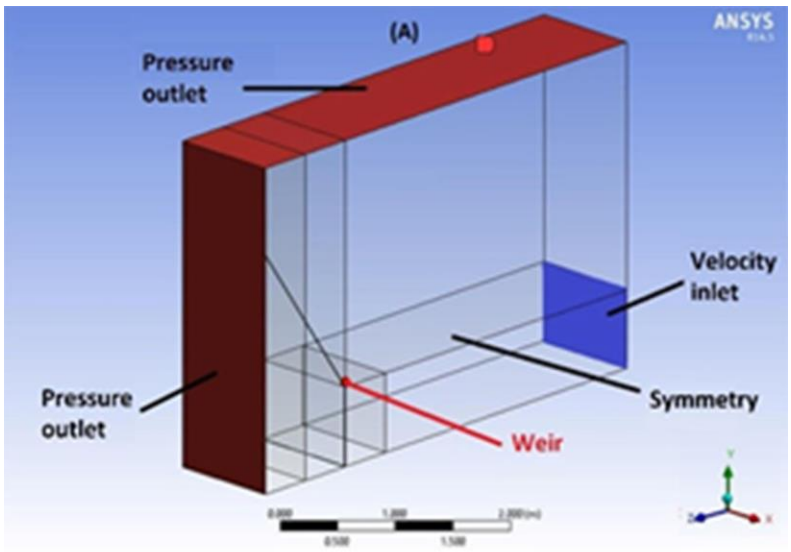

Figure 3. Boundary conditions.

After the generation of geometry, the domain is divided into a sufficient number of cells or elements that do not overlap and cover all the geometry, where general conservation equations were applied. Meshing module was used to generate mesh in the model, for spatial discretization, it was decided to employ a predominantly hexahedral mesh; among the advantages of hexahedral meshing is the reduction of the number of domain elements and the improvement of the convergence of the solution (Sánchez & Elsitidié, 2011). The most important parameter to define de viability of the computational model is the relationship between experimental and simulate data.

The boundary conditions of the computational model are established (Table 3). The flow inlet condition is located upstream of the weir at a minimum distance of two times the width of the channel (Boss, Replogle, & Clemmens, 1984) to avoid that the hydraulic load is not affected by the flow approach condition, the most common inlet condition in open channels is the mean flow velocity (inlet velocity) obtained from the flow rate and the continuity equation; the vertical plane located downstream of the spillway is defined as the free outlet of the flow to the atmosphere, the outlet condition assigned for open channels is atmospheric pressure (outlet pressure); as the computational model is symmetric in the axis of the spillway, the condition of symmetry is assigned in the lateral planes perpendicular to the axis of the spillway; the weir, the platform and the lateral walls of the channel are defined as solid stationary and non-slip with the roughness of $1.6*10^{-9}$m (roughness of high-density polyethylene).

Table 3. Boundary conditions (Figure 3).

Boundary conditions	
Input	Velocity inlet (upstream) Atmospheric pressure (upper area of the channel)
Output	Atmospheric pressure (downstream)
Solid	Weir Side walls and channel platform

Tecnología y ciencias del agua, ISSN 2007-2422, 12(4), 112-162. DOI: 10.24850/j-tyca-2021-04-03

Symmetry	Side boundary and perpendicular plane to the axis of the weir

The basis of an adjusted and adequate development to the physical conditions of a computational model is the numerical scheme that approximately solves the equations that describe the flow. Because it is a two-phase (water-air) and free surface flow, it is assigned to the multiphase *VOF* model and the turbulence *K*-ε (Launder & Spalding, 1974) model because it is the most complete simple method with the lowest computational cost to simulate turbulence demonstrating its advantage in confined and internal flows (Fernández, 2012) and in free-surface flows (Chanel & Doering, 2008; Olsen, Nils, & Kjellesvig, 1998; Jiang, Diao, Sun, & Ren, 2018).

The pressure-velocity coupling of the SIMPLE algorithm was used (Semi-Implicit Method for Pressure Linked Equations), it approaches convergence through a series of intermediate fields of pressure and velocity which satisfies continuity (Fernández, 2012). The use of the "Upwind" spatial discretization system ensures stable schemes, but its first-order characteristic makes it sensitive to numerical diffusion errors. Such errors can be minimized using higher-order discretization schemes.

Several simulations were performed to evaluate the precision of the model according to the previous results reported in the bibliography. Statistical methods were used to compare simulated results with experimental and analytical results. As an indicator of the quality of measurement of numerical results, the relative percentage error was

used, which indicates how far from the experimental value is from the numerical estimation with CFD and it is defined with Equation (16):

$$\text{relative percentage error} = \frac{\text{Simulated} - \text{experimental}}{\text{experimental}} * 100 \quad (16)$$

Table 4 shows simulation scenarios according to experimental conditions.

Table 4. Simulation scenarios.

Weir	Experimental conditions					
	Channel width (m)	**Width of rectangular section b_1 (m)**	**Width of triangular section b_2 (m)**	**Notch angle θ (°)**	**Load h (m)**	**Flow rates Q (l s^{-1})**
Rectangular	2.00	1.00	-	-	0.27	249.00
Triangular	2.00	-	2.00	90	0.50	246.00
Compound	1.49	0.25	0.20	90	0.113	8.06
		0.25	0.20	90	0.131	14.36
		0.25	0.20	90	0.136	16.33
		0.40	0.20	90	0.122	13.35
		0.40	0.20	90	0.141	23.35
		0.40	0.20	90	0.169	45.50

0.50	0.20	90	0.110	8.06
0.50	0.20	90	0.123	14.36
0.50	0.20	90	0.127	16.33

Results are analyzed and they are exposed in a qualitatively (maps, distributions, vectors) and quantitatively (graphs, integrals, values, averages) way.

Results analysis and discussion

Evaluation of the numerical model

Table 5 reports the simulation parameters and shows the statistical comparison of the experimental results reported by Sotelo (1997) with those simulated with CFD. The discharge coefficients of the rectangular and triangular weirs were obtained from Equation (4) and Equation (5), respectively.

Table 5. Hydraulic variables and relative percentage errors between experimental and numerical values of the rectangular and triangular weirs.

Weir	Method	Load *h* (m)	Notch angle θ (°)	Discharge coefficient C_d	Flow rates *Q* (l s^{-1})
Rectangular	Experimental	0.270	-	0.6017	249
	CFD	0.271	-	0.6016	251
	Relative error (%)	0.37	-	-0.01	0.66
Triangular	Experimental	0.500	90	0.5902	246
	CFD	0.499	90	0.5902	245
	Relative error (%)	-0.2	-	0.00	-0.30

According to the results, the CFD model simulates both weirs very well. Although the CFD model predicted in the best way the discharge flow in a triangular weir than in the case of the rectangular weir, the relative error of the triangular weir is slightly less than the case of the rectangular weir. The use of the triangular weir is recommended for flow rates lower than 30 l s^{-1}, however, Sotelo (1997) also documents that its accuracy is greater than a rectangular weir even for flow rates of 30 to 300 l s^{-1}.

Once the CFD model was evaluated, nine scenarios were simulated for the combined weir, which are statistically compared with the experimental results reported by Jan *et al*. (2006). The discharge coefficients, C_{dt} and C_{dr}, of the triangular and rectangular sections of the compound weir are

calculated with Equation (7) and Equation (8). Table 6 reports the flow rates obtained numerically for the three sections of compound weirs.

Table 6. Coefficients of discharge and numerical flow rates in compound weirs obtained by means of the CFD tool.

Notch angle θ (°)	Rectangular section width b_1 (m)	Triangular section width b_2 (m)	Load on rectangular section CFD h_1 (m)	Load on triangular section CFD h_2 (m)	Discharge coefficient in rectangular section C_{dr}	Discharge coefficient in triangular section C_{dt}	CFD Flow rates Q (l s^{-1})
90	0.25	0.20	0.014	0.114	0.590	0.579	8.08
90	0.25	0.20	0.033	0.133	0.591	0.579	14.31
90	0.25	0.20	0.040	0.140	0.591	0.579	16.31
90	0.40	0.20	0.028	0.128	0.594	0.579	13.27
90	0.40	0.20	0.042	0.142	0.594	0.579	23.24
90	0.40	0.20	0.079	0.179	0.596	0.579	45.30
90	0.50	0.20	0.010	0.110	0.595	0.579	8.11
90	0.50	0.20	0.025	0.125	0.596	0.579	14.47
90	0.50	0.20	0.029	0.129	0.597	0.579	16.33

The relative errors, calculated with Equation (16), are presented in Table 7; the analytical flow rates (obtained with Equation (6)) and the numerical flow rates (obtained in CFD) are compared against the experimental flow rates.

Tecnología y ciencias del agua, ISSN 2007-2422, 12(4), 112-162. DOI: 10.24850/j-tyca-2021-04-03

Table 7. Relative errors of analytical and numerical flow rates versus experimental flow rates.

Rectangular section width b_1(m)	Experimental flow rates Q (ls^{-1})	Analytical flow rates Q ($l\ s^{-1}$)	CFD flow rates Q ($l\ s^{-1}$)	Relative error analytical *vs*. experimental (%)	Relative error CFD *vs*. Experimental (%)
0.25	8.06	7.13	8.08	-11.49	0.21
0.25	14.36	13.02	14.31	-9.33	-0.35
0.25	16.33	14.95	16.31	-8.47	-0.14
0.40	13.35	11.59	13.27	-13.21	-0.59
0.40	23.35	21.41	23.24	-8.30	-0.46
0.40	45.50	39.90	45.30	-12.30	-0.44
0.50	8.06	7.23	8.11	-10.28	0.65
0.50	14.36	13.30	14.47	-7.41	0.74
0.50	16.33	15.53	16.33	-4.93	0.00

Estimate of discharge coefficient

Tecnología y ciencias del agua, ISSN 2007-2422, 12(4), 112-162. DOI: 10.24850/j-tyca-2021-04-03

The discharge equation of the compound weir (Equation (6)) can be rewritten as a function of a single discharge coefficient (Equation (17)):

$$Q = C_d(2g)^{0.5}\left[\frac{4}{3}b_1h_1^{1.5} + \frac{8}{15}\tan\theta/_2\,(h_2^{2.5} - h_1^{2.5})\right] \quad (17)$$

Equating Equation (7) and Equation (17) it is possible to obtain a single discharge coefficient (Equation (18)).

$$C_d = \frac{C_{dr}\frac{4}{3}b_1h_1^{1.5} + C_{dt}\frac{8}{15}\tan\theta/_2(h_2^{2.5} - h_1^{2.5})}{\frac{4}{3}b_1h_1^{1.5} + \frac{8}{15}\tan\theta/_2(h_2^{2.5} - h_1^{2.5})} \quad (18)$$

The discharge coefficient of the rectangular section (C_{dr}) is calculated with Equation (4) and that of the triangular section (C_{dt}) is obtained with Equation (7). Equation (4) considers the geometry of the weir and the load of the rectangular section, while Equation (7) is independent of the load and its value is constant for each angle of the notch, and the effects of surface tension and viscosity are especially negligible.

Equation (18) is only valid for loads greater than h_1, that is, $h2 > h1$. The discharge coefficients in Table 8 are calculated with Equation (18) for values of $h_2 / P \leq 1$.

Table 8. Discharge coefficient calculation.

Tecnología y ciencias del agua, ISSN 2007-2422, 12(4), 112-162. DOI: 10.24850/j-tyca-2021-04-03

θ (°)	Channel width (m)	P (m)	b_1 (m)	b_2 (m)	h_1 (m)	h_2 (m)	C_d	h_2/P
90	1.49	0.2	0.25	0.20	0.013	0.113	0.634	0.565
90	1.49	0.2	0.25	0.20	0.031	0.131	0.626	0.655
90	1.49	0.2	0.25	0.20	0.036	0.136	0.623	0.68
90	1.49	0.2	0.25	0.20	0.02	0.12	0.632	0.60
90	1.49	0.2	0.25	0.20	0.06	0.16	0.613	0.80
90	1.49	0.2	0.25	0.20	0.10	0.20	0.603	1.00
90	1.49	0.2	0.40	0.20	0.022	0.122	0.655	0.61
90	1.49	0.2	0.40	0.20	0.041	0.141	0.641	0.705
90	1.49	0.2	0.40	0.20	0.069	0.169	0.629	0.845
90	1.49	0.2	0.40	0.20	0.01	0.11	0.662	0.55
90	1.49	0.2	0.40	0.20	0.08	0.18	0.626	0.90
90	1.49	0.2	0.40	0.20	0.10	0.20	0.622	1.00
90	1.49	0.2	0.50	0.20	0.01	0.110	0.680	0.55
90	1.49	0.2	0.50	0.20	0.023	0.123	0.669	0.615
90	1.49	0.2	0.50	0.20	0.027	0.127	0.665	0.635
90	1.49	0.2	0.50	0.20	0.04	0.14	0.656	0.70
90	1.49	0.2	0.50	0.20	0.06	0.16	0.647	0.80
90	1.49	0.2	0.50	0.20	0.10	0.20	0.639	1.00

Tecnología y ciencias del agua, ISSN 2007-2422, 12(4), 112-162. DOI: 10.24850/j-tyca-2021-04-03

The discharge coefficients in Table 8 are presented as a function of the ratio h_2/P (Figure 4) and are adjusted to Equation (19) to facilitate the design of the weir.

$$C_d = a_1 + a_2 \cos\left(d * {}^{h_2}/_{P}\right) + a_3 \sin\left(d * {}^{h_2}/_{P}\right) + a_3 \cos\left(2d * {}^{h_2}/_{P}\right) + a_4 \sin\left(2d * {}^{h_2}/_{P}\right) \quad (19)$$

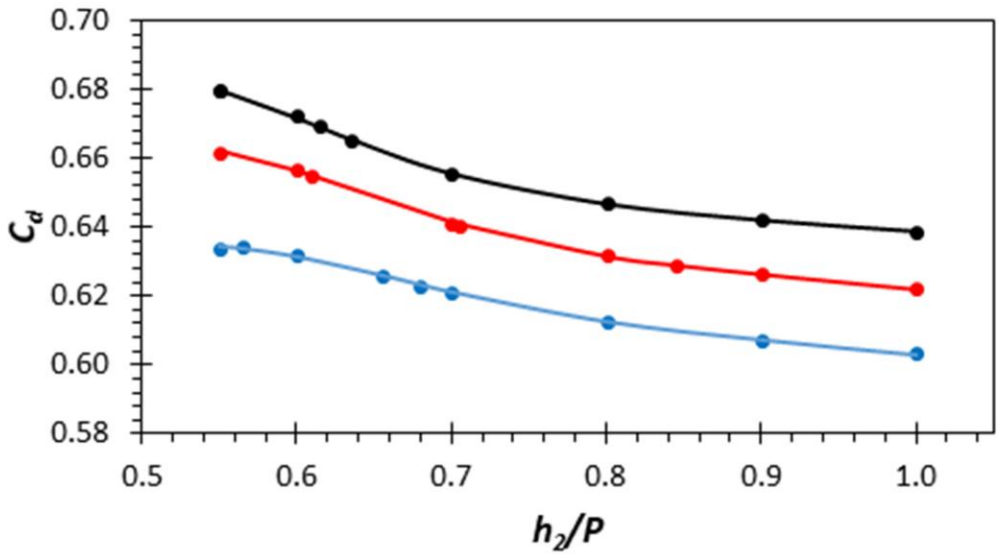

Figure 4. C_d *vs*. h_2 / P; b_1 = ●, b_2 = ●, b_3 = ●.

The coefficients of Equation (19) are calculated with equations (20)-(25).

Tecnología y ciencias del agua, ISSN 2007-2422, 12(4), 112-162. DOI: 10.24850/j-tyca-2021-04-03

$$a_1 = 76.96 * 10^{-3}\left[2\left(b_1 + \tan\frac{\theta}{2}\{h_2 - h_1\}\right)\right]^2 - 18.18 * 10^{-2}\left[2\left(b_1 + \tan\frac{\theta}{2}\{h_2 - h_1\}\right)\right] + 69.12 * 10^{-2} \quad (20)$$

$$a_2 = 7.4 * 10^{-5}\left[2\left(b_1 + \tan\frac{\theta}{2}\{h_2 - h_1\}\right)\right]^2 + 29.98 * 10^{-3}\left[2\left(b_1 + \tan\frac{\theta}{2}\{h_2 - h_1\}\right)\right] - 27.86 * 10^{-3} \quad (21)$$

$$a_3 = 90.28 * 10^{-3}\left[2\left(b_1 + \tan\frac{\theta}{2}\{h_2 - h_1\}\right)\right]^2 - 79.24 * 10^{-3}\left[2\left(b_1 + \tan\frac{\theta}{2}\{h_2 - h_1\}\right)\right] + 63.36 * 10^{-4} \quad (22)$$

$$a_4 = -77.41 * 10^{-4}\left[2\left(b_1 + \tan\frac{\theta}{2}\{h_2 - h_1\}\right)\right]^2 - 19.82 * 10^{-4}\left[2\left(b_1 + \tan\frac{\theta}{2}\{h_2 - h_1\}\right)\right] + 60.47 * 10^{-4} \quad (23)$$

$$a_5 = -39.37 * 10^{-3}\left[2\left(b_1 + \tan\frac{\theta}{2}\{h_2 - h_1\}\right)\right]^2 + 34.93 * 10^{-3}\left[2\left(b_1 + \tan\frac{\theta}{2}\{h_2 - h_1\}\right)\right] - 56.38 * 10^{-4} \quad (24)$$

$$d = 6.981 \quad (25)$$

It was used as a criterion to evaluate the quality of the equations (19)-(25) the coefficient of determination (R^2), the coefficient R^2 allows to measure the agreement between two linearly related values. The

Tecnología y ciencias del agua, ISSN 2007-2422, 12(4), 112-162. DOI: 10.24850/j-tyca-2021-04-03

values of the coefficient R^2 of equations (19)-(25) is 0.999, which allows us to conclude that there is a high degree of concordance between the measured and calculated values. Finally, the flow rates that pass over the weir and the new discharge coefficients obtained with the equations (19)-(25) are shown in Table 9.

Table 9. Calculation of the flow rates and the discharge coefficient.

θ (°)	Channel width (m)	b_1 (m)	b_2 (m)	h_1 (m)	h_2 (m)	C_d	Analytical flow rates Q (l s^{-1})	Experimental flow rates Q (l s^{-1})
90	1.49	0.25	0.20	0.013	0.113	0.634	7.79	8.06
90	1.49	0.25	0.20	0.031	0.131	0.626	14.00	14.36
90	1.49	0.25	0.20	0.036	0.136	0.623	15.99	16.33
90	1.49	0.40	0.20	0.022	0.122	0.655	13.01	13.35
90	1.49	0.40	0.20	0.041	0.141	0.641	23.40	23.35
90	1.49	0.40	0.20	0.069	0.169	0.629	42.56	45.50
90	1.49	0.50	0.20	0.01	0.110	0.680	8.45	8.06
90	1.49	0.50	0.20	0.023	0.123	0.669	15.18	14.36
90	1.49	0.50	0.20	0.027	0.127	0.665	17.61	16.33

Discussion

Tecnología y ciencias del agua, ISSN 2007-2422, 12(4), 112-162. DOI: 10.24850/j-tyca-2021-04-03

Results revealed that the flow rates obtained through the CFD tool better predict the discharge than the analytical flow rates. Analytically there is inaccuracy of the discharge measurement during the transition between geometric sections, that is, in the region where the discharge exceeds the boundary between the triangular and rectangular sections. Lee, Chan, Huang, and Leu (2012) mentioned that the discharge discontinuity during the transition is associated with changes in mass and momentum; these are effects of variables, of conservation equations, which are not considered in the theoretical equations for the measurement of flow rates, as are the effects of viscosity and velocity distribution in proximity to the weir.

To improve the fit of the analytical model, Jan, Chang, and Kuo (2009) proposed an adjustment factor α, which multiplies the analytically calculated flow rates to estimate the discharge flow. α is defined as the average of ratio of experimental flow rates to the analytical flow rates (α was not considered in the results of Table 8). The adjustment value was $\alpha = 1.11$, which indicates that the analytical method is undervalued concerning the experimental results.

The difficulty of describing the flow in the transition zone between the triangular and rectangular sections is well known. CFD must assume hypotheses to simulate and test sub-models to describe the flow, such as turbulence and phase change. Flow rates are very similar in several

Tecnología y ciencias del agua, ISSN 2007-2422, 12(4), 112-162. DOI: 10.24850/j-tyca-2021-04-03

scenarios. Under these conditions, CFD simulations will allowed to know in detail the behavior of the flow in critical sections of the weir.

Hydraulic analysis of the coefficient of discharge

The proposed equations for obtaining the discharge coefficient (equations (19)-(25)) made it possible to analytically predict the flow rates of the compound weir, these equations consider the geometry of the weir (width, height, angle, and height of the triangular notch, width of the rectangular section) and the level of static charge. Table 10 compares the analytical flow rates with the experimental flow rates, the relative errors between both flow rates vary from 0.2 % to 7.8 %, the results of the flow rates obtained analytically from the discharge coefficient are acceptable.

Table 10. Comparison between analytical and experimental flow rates.

C_d	Analytical flow rates Q (l s^{-1})	Experimental flow rates Q (l s^{-1})	Relative error (%)
0.634	7.79	8.06	-3.36
0.626	14.00	14.36	-2.50
0.623	15.99	16.33	-2.06

Tecnología y ciencias del agua, ISSN 2007-2422, 12(4), 112-162. DOI: 10.24850/j-tyca-2021-04-03

0.655	13.01	13.35	-2.59
0.641	23.40	23.35	0.22
0.629	42.56	45.50	-6.47
0.680	8.45	8.06	4.82
0.669	15.18	14.36	5.72
0.665	17.61	16.33	7.80

The graph in Figure 4 shows that the weirs have a higher discharge coefficient for small hydraulic loads $h_2 / P < 0.6$ and increasing the width of the rectangular section. The reduction of the discharge coefficient values in the weir $b_1 = 0.25$ m is smooth compared to the other weirs, from $h_2 \approx 0.7$ values the slope of the coefficient discharge curve of weirs $b_1 = 0.40$ m and $b_1 = 0.50$ m is softer and tends to stabilize from $h_2 / P \geq 1$. It is possible that at the $h_2 / P \approx 0.7$ inflection point where the change in the slope occurs, it is due to the presence of the pressure difference between the triangular and rectangular sections as well as the variation in the velocity of the discharge flow. Although the proposed discharge coefficient equation allows a better prediction of the flow rates, the results are not accurate to the experimental values, the charge-discharge relationship is directly affected by the discontinuity of the flow for loads above the horizontal crest of the weir (Lee *et al*., 2012).

Tecnología y ciencias del agua, ISSN 2007-2422, 12(4), 112-162. DOI: 10.24850/j-tyca-2021-04-03

Nappe characteristics

In the compound weir there are two nappes (Figure 5) as a consequence of the pressure difference that exists during the discharge in the triangular and rectangular sections (Figure 6). On the other hand, the rectangular section presents subatmospheric pressures and lower discharge speed, while in the triangular section there are pressures greater than the atmosphere and higher discharge velocity together with a nappe thicker than that of the rectangular section (Figure 5). The CFD tool allows to identify the presence of depression in the surface free of the water as a consequence of the high discharge speed generated in the triangular zone of the compound weir (Figure 7).

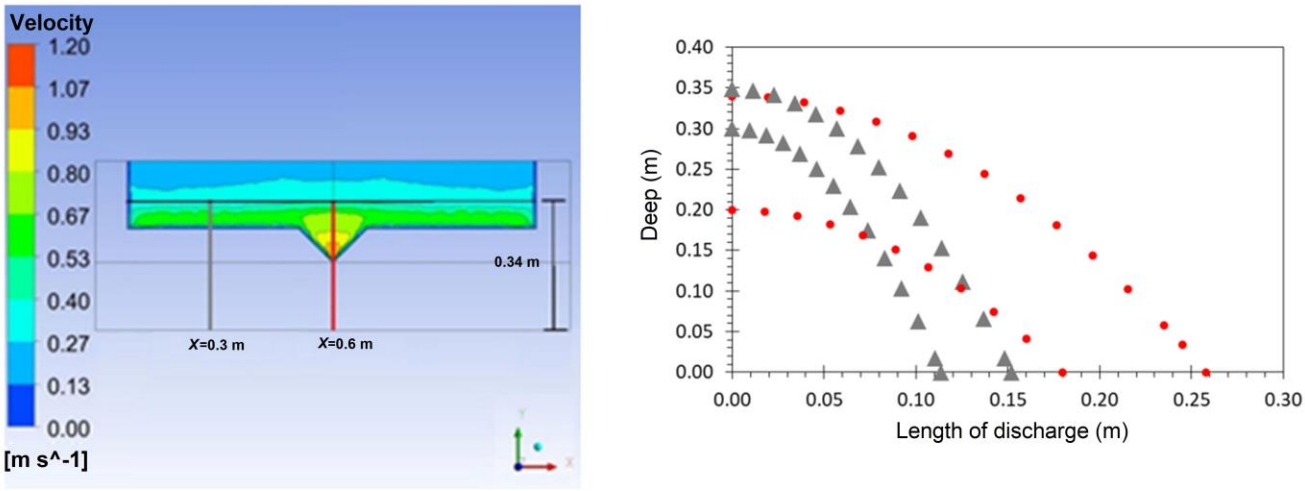

Figure 5. Particle tracking monitoring during discharge: ▲ X = 0.3 m, ● X = 0.6 m; b_1 = 0.40 m; Q = 23.35 l s^{-1}

Tecnología y ciencias del agua, ISSN 2007-2422, 12(4), 112-162. DOI: 10.24850/j-tyca-2021-04-03

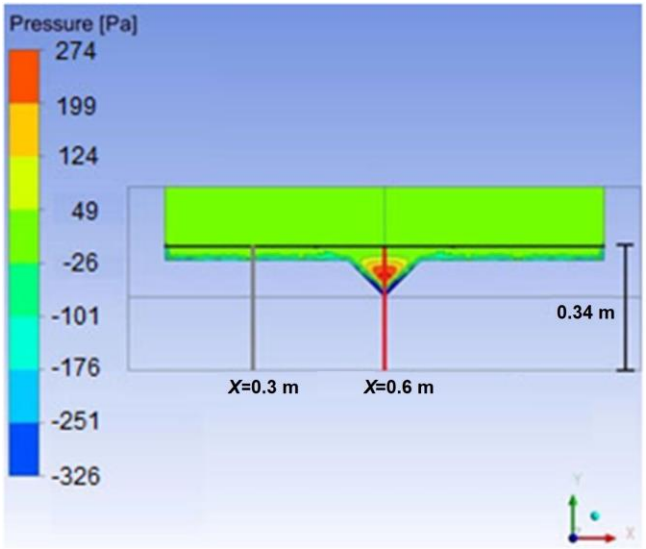

Figure 6. Relative pressures: b_1 = 0.40 m; Q = 23.35 l s^{-1}; X in meters; ——— x = 0.3; ——— x = 0.6; ——— free surface.

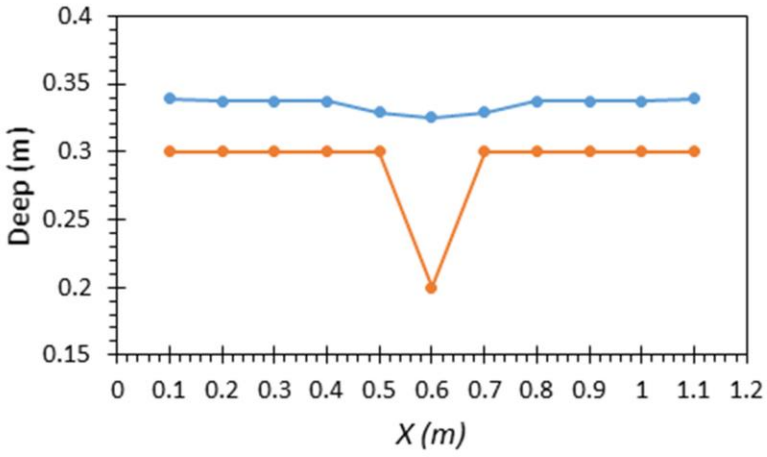

Figure 7. Profile of the free surface during discharge. Free surface———, weir edge———; b_1 = 0.40 m; Q = 45.30 l s^{-1}.

Tecnología y ciencias del agua, ISSN 2007-2422, 12(4), 112-162. DOI: 10.24850/j-tyca-2021-04-03

Speed measurements were made, its behavior is affected by the hydraulic load and the geometry of the compound weir. An important consequence of the distribution of the velocity field (Figure 8) is the impact on the discharge in certain sections of the weir. In general, the speed contours of the rectangular section are presented almost parallel to the crest of the weir. The velocities near the sloping regions of the crest triangular are lower than the rest of the triangular section, near the bottom of that section the velocity is relatively high, the length of the discharge flow in that area is greater relative to the other areas of the weir. The velocity profiles in Figure 8 present velocity gradients at the transition from the triangular to the rectangular section called the mixing zone (Lee *et al*., 2012), the velocity gradients decrease, and the velocities in the mixing zone increase as increases the hydraulic load. The velocity profile along the width of the channel (Figure 8) shows a reduction in discharge speed before approaching the triangular section, this phenomenon (red circle) is more visible for small loads on the rectangular section (Y = 0.31 m) and it is possible that it is due to the discontinuity of the flow near the mixing zone where according to Lee *et al*. (2012) presents mass and momentum exchange, for higher loads the speed reduction is less abrupt and with a tendency to stabilize (Y = 0.34 m).

Tecnología y ciencias del agua, ISSN 2007-2422, 12(4), 112-162. DOI: 10.24850/j-tyca-2021-04-03

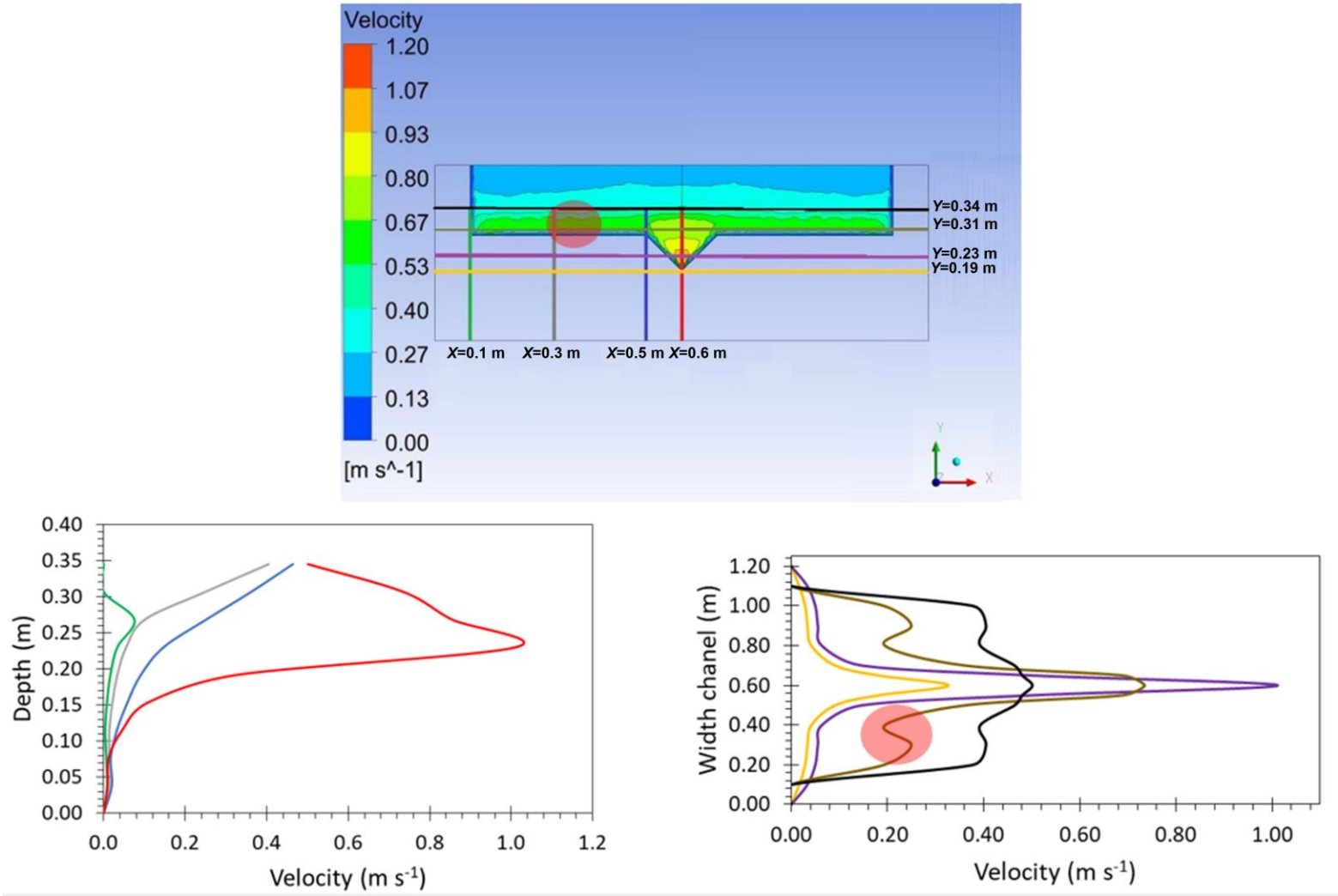

Figure 8. Velocity profiles: b_1 = 0.40 m; Q = 23.35 l s^{-1}; X in meters; X = 0.1; X = 0.3; X = 0.5; X = 0.6; Y = 0.19; Y = 0.23; Y = 0.31; Y = 0.34

Conclusions

Tecnología y ciencias del agua, ISSN 2007-2422, 12(4), 112-162. DOI: 10.24850/j-tyca-2021-04-03

The experimental and analytical studies reported in the bibliography allowed to reproduce numerically, by CFD simulations, the hydraulic behavior of compound (rectangular-triangular) sharp-crest weirs. Based on the objective of this work, as well as the results achieved, it is worth noting that the flow rates obtained numerically are statistically in agreement with their experimental values. Furthermore, it has been possible to improve the estimation of the analytically obtained flows. Therefore, the main conclusions of this study can be summarized as:

1. There is an error of up to 7.8 % in the discharge flow estimate with an analytical calculation compared to the laboratory flow measurements, and the error is reduced to 0.74 % when the estimate is made with CFD.
2. Regarding weir design, an expression of the global discharge coefficient was proposed as a function of the h_2/P ratio and the weir geometry. Furthermore, the simulation results reveal that the value and the variation of the discharge coefficient increase with the increasing width of the rectangular section (b_1). In fact, the discharge coefficient values are higher for ratios $h_2 / P < 0.6$ and from $h_2/P \geq 1$ it tends to stabilize. From $h_2 / P \approx 0.7$ the decrease in the discharge coefficient values is less drastic as a consequence of the reduction of the speed gradients that occur in the mixing zone and the pressure difference.
3. It was also possible to characterize the water nappe. CFD allowed identifying sub-atmospheric pressure in the rectangular region, while in

Tecnología y ciencias del agua, ISSN 2007-2422, 12(4), 112-162. DOI: 10.24850/j-tyca-2021-04-03

the triangular zone the pressure is higher than atmospheric. In addition, during discharge, a thick nappe was observed in the area dominated by the triangular section and depression in the surface free. The speed distribution was characterized, the speed contours of the rectangular section are almost parallel to the crest of the weir, in the lower area of the triangular section there are high discharge speeds than in the rest of the weir where the nappe is more thickness and depression in the free surface is originated, the speed gradients that present during the transition from the triangular to the rectangular section decrease with the increase of the hydraulic load and the speeds in the mixing zone increases. In the rectangular section, the speed reduction was observed and later the sudden increase near the area dominated by the triangular section this caused by the discontinuity of the flow and the proximity to the mixing area, the speed increases and tends to stabilize as the hydraulic load increases.

4. According to the results obtained, it is possible to assume that the analytical error in the estimation of the discharge flow is due to the variation of the discharge velocity in the transition from the triangular section to the rectangular one and discontinuity of the flow.

5. Finally, the results allow us to conclude, on the one hand, that a triangular-rectangular compound weir largely satisfies the precision required to efficiently deliver water to irrigation users considering the important variation of delivery of water volumes. On the other hand, the experimentation and modeling with CFD are complementary strategies to understand and analyze details of the hydraulic operation of compound weirs.

Acknowledges

This work is part of the Autor Ph.D. Thesis Erick Dante Mattos Villarroel, in the graduate program of Engineering and Water Sciences, from the Mexican Institute of Water Technology (IMTA)

Nomenclature

B = channel width.

B = weir width.

b_1 = width of the rectangular section of the compound weir.

b_2 = width of the triangular section of the compound weir.

C_d = coefficient of discharge.

C_{dr} = coefficient of discharge of the section rectangular the compound weir.

C_{dt} = coefficient of discharge of the section triangular the compound weir.

C_μ, $C_{1\varepsilon}$, $C_{2\varepsilon}$ = constants of turbulent model K-Ɛ.

f = forces of the body per unit mass.

g = acceleration of gravity.

h = static load on the weir.

h_1 = static load on the section rectangular the compound weir.

h_2 = static load on the section triangular the compound weir.

K = turbulent kinetic energy.

k = coefficient depending on the dimensions and shape of the weir.

n = dimensionless number depending on the shape of the weir.

$\dot{m}_{pq}$ = mass transfer from phase p to phase q.

$\dot{m}_{qp}$ = the mass transfer from phase q to phase p.

P = height of the weir.

P_K = turbulent generation due to the viscous force.

P_{kb}, $P_{\varepsilon b}$ = influence of floatability force.

p = dynamic pressure.

Q = dischage over weir.

q^{th} = phase q.

S_{α_q} = term source.

U = velocity field.

α_q = volume fraction of the phase q.

$\acute{\varepsilon}$ = dispersion of turbulent kinetic energy.

θ = notch angle of the triangular weir.

μ = dynamic viscosity.

Tecnología y ciencias del agua, ISSN 2007-2422, 12(4), 112-162. DOI: 10.24850/j-tyca-2021-04-03

μ_t = turbulent viscosity.

ρ = density of the fluid.

ρ_q = density of the phase q.

σ_k, σ_ε = constants of turbulent model K-ε.

References

ASTM, American Society for Testing and Materials. (1993). *Standard method for open-channel flow measurement of water with thin-plate weirs* (ASTM D5242). West Conshohocken, USA: American Society for Testing and Materials. Recovered from https://allcivilstandard.com/wp-content/uploads/2018/12/D-5242.pdf

Aydin, I., Altan-Sakarya, A. B., & Sisman, C. (2011). Discharge formula for rectangular Sharp-crested weirs. *Flow Measurement and Instrumentation*, 22(2), 144-151. DOI: 10.1016/j.flowmeasinst.2011.01.003

Bagheri, S., & Heidarpour, M. (2009). Flow over rectangular sharp crested weirs. *Irrigation Science*, 28(2), 173-179. DOI: 10.1007/s00271-009-0172-1

Bautista, C., Robles, O., Júnez, F. H., & Playán, E. (2013). Discharge coefficient analysis for triangular sharp-crested weirs using low-speed photographic technique. *Journal of Irrigation and Drainage Eng*ineering, 140(3), 06013005. DOI: 10.1061/(ASCE)IR.1943-4774.0000683

Bos, M. G. (1989). *Discharge measurement structures* (3rd revised edition). Wageningen, The Netherlands: International Institute for Land Reclamation and Improvement. Recovered from https://www.samsamwater.com/library/pub20.pdf

Bos, M. G., Replogle, J. A., & Clemmens, A. J. (1984). *Flow measuring flumes for open channel systems*. New York, USA: John Wiley & Sons.

BSI, British Standards Institution. (1965). *BSI 3680-4A. Thin-plate weirs and venture flumes in methods of measurement of liquid flow in open channel. Part 4A*. London, UK. DOI: 10.3403/01558628U

Chanel, P. G., & Doering, J. C. (2008). Assessment of spillway modelling using computational fluid dynamics. *Canadian Journal of Civil Engineering*, 35(12), 1481-1485. DOI: 10.1139/l08-094

Chen, Y., Fu, Z., Chen, Q., & Cui, Z. (2018). Discharge coefficient of rectangular short-crested weir with varying slope coefficients. *Water*, 10(2), 204. DOI: 10.3390/w10020204

Clemmens, A. J., Wahl, T. L., Bos, M. G., & Replogle, J. A. (2001). *Water measurement with flumes and weirs* (Publication 58). Wageningen, The Netherlands: International Institute for Land Reclamation and Improvement/ILRI. Recovered from https://library.wur.nl/WebQuery/wurpubs/fulltext/82325

Duró, G., Dios, M. D., López, A., Liscia, S. O., & Angulo, M. A. (September, 2012). Comparación de simulaciones en CFD y modelación física de una central hidrocombinada. In: *XXIV Congreso Latinoamericano de Hidráulica*. San José de Costa Rica, Costa Rica. DOI: 10.13140/RG.2.1.3880.8406

El-Alfy, K. S. (2005). Effect of vertical curvature of flow at weir crest on discharge coefficient. In: *The 9th International Water Technology Conference*. Sharm El-Sheikh, Egypt. Recovered from https://pdfs.semanticscholar.org/83f8/4250668c383dd5121cf56e343f41d42902e3.pdf?_ga=2.137244208.1604846566.1576367520-1959585653.1576367520

Emiroglu, M. E., Kaya, N., & Agaccioglu, H. (2010). Discharge capacity of labyrinth side weir located on a straight channel. *Journal of Irrigation Drainage Engineering*, 136(1), 37-46. DOI: 10.1061/(ASCE)IR.1943-4774.0000112

Fernández, J. M. (2012). *Técnicas numéricas en ingeniería de fluidos: introducción a la dinámica de fluidos computacional (CFD) por el método de volumen finito*. Barcelona, España: Reverté.

Fu, Z. F., Cui, Z., Dai, W. H., & Chen, Y. J. (2018). Discharge coefficient of combined orifice-weir flow. *Water*, 10(6), 699. DOI: 10.3390/w10060699

Henderson, F. M. (1966). *Open channel flow*. New York, USA: MacMillan Publishing Co., Inc. Recovered from https://heidarpour.iut.ac.ir/sites/heidarpour.iut.ac.ir/files//u32/open-henderson.pdf

Hirt, C. W., & Nichols, B. D. (1981). Volume of fluid (VOF) method for the dynamics of free boundaries. *Journal of Computational Physics*, 39(1), 201-225. DOI: 10.1016/0021-9991(81)90145-5

Ho, D. K., Boyes, K. M., & Donohoo, S. M. (December, 2001). Investigation of spillway behavior under increased maximum flood by computational fluid dynamics technique. *Procedures. 14th*

Australasian Fluid Mechanics Conference. Adelaide University, Adelaide, Australia. Recovered from https://people.eng.unimelb.edu.au/imarusic/proceedings/14/fm010091.pdf

Ho, D. K., Boyes, K. M., Donohoo, S. M., & Cooper, B. (October, 2003). Numerical flow analysis for spillways. *Procedures. 43rd ANCOLD Conference*. Hobart, Tasmania. Recovered from https://www.flow3d.com/wp-content/uploads/2014/08/Numerical-Flow-Analysis-for-Spillways.pdf

ISO, International Organization for Standardization. (1980). ISO 1438/1-1980(E), *Water flow measurement in open channels using weirs and venturi flumes. Part 1: Thin plate weirs*. International Organization for Standardizatio Geneva, Switzerland.

Jan, C. D., Chang, C. J., & Kuo, F. H. (2009). Experiments on discharge equations of compound broad-crested weirs. *Journal of Irrigation and Drainage Engineering*, 135(4), 511-515. DOI: 10.1061/(ASCE)IR.1943-4774.0000019

Jan, C. D., Chang, C. J., & Lee, M. H. (2006). Discussion of "Design and calibration of a compound sharp-crested weir" by Martinez, J., Reca, J., Morillas, M. T., & López, J. G. *Journal of Hydraulic Engineering*, 132(8), 868-871. DOI: 10.1061/(ASCE)0733-9429(2006)132:8(868)

Jiang, L., Diao, M., Sun, H., & Ren, Y. (2018). Numerical modeling of flow over a rectangular broad-crested weir with a sloped upstream face. *Water*, 10(11), 1663. DOI: 10.3390/w10111663

Jones, W. P., & Launder, B. E. (1972). The prediction of laminarization with a two-equation model of turbulence. *International Journal of Heat Mass Transfer*, 15(2), 301-314. DOI: 10.1016/0017-9310(72)90076-2

Kumar, S., Ahmad, Z., & Mansoor, T. (2011). A new approach to improve the discharging capacity of sharp-crested triangular plan form weirs. *Flow Measurement and Instrumentation*, 22(3), 175-180. DOI: 10.1016/j.flowmeasinst.2011.01.006

Launder, B. E., & Spalding, D. B. (1974). The numerical computation of turbulence flows. *Computer Methods in Applied Mechanics and Engineering*, 3(2), 269-289. DOI: 10.1016/0045-7825(74)90029-2

Lee, J. T., Chan, H. C., Huang, C. K., & Leu, J. M. (2012). Experiments on hydraulic relations for flow over a compound sharp-crested weir. *International Journal of Physical Sciences*, 7(14), 2229-2237. DOI: 10.5897/IJPS11.1695

Negm, A. A., Al-Brahim, A. M., & Alhamid, A. A. (2002). Combined-free flow over weirs and below gates. *Journal of Hydraulic Research*, 40(3), 359-365. DOI: 10.1080/00221680209499950

Olsen, N. R., Nils, R. B., & Kjellesvig, H. M. (1998). Three-dimensional numerical flow modeling for estimation of spillway capacity. *Journal Hydraulic Research*, 36(5), 775-784. DOI: 10.1080/00221689809498602

Rady, R. M. A. (2011). 2D-3D modeling of flow over sharp-crested weirs. *Journal of Applied Sciences Res*earch, 7(12), 2495-2505. Recovered

from https://www.flow3d.com/wp-content/uploads/2014/08/2D-3D-Modeling-of-Flow-Over-Sharp-Crested-Weirs.pdf

Sánchez, J. M. C., & Elsitdié, L. G. C. (mayo, 2011). Consideraciones del mallado aplicadas al cálculo de flujos bifásicos con las técnicas de dinámica de fluidos computacional. *Jornada de Introducción a la Investigación de la UPCT*. Universidad Politécnica de Cartagena, Fuente Álamo, España. Recovered from https://www.researchgate.net/profile/Luis_Castillo26/publication/277210544_Consideraciones_del_mallado_aplicadas_al_calculo_de_flujos_bifasicoscon_las_tecnicas_de_dinamica_de_fluidos_computacional/links/55a7f20808ae815a042129f3/Consideraciones-del-mallado-aplicadas-al-calculo-de-flujos-bifasicoscon-las-tecnicas-de-dinamica-de-fluidos-computacional.pdf

Shen, J. (1981). *Discharge characteristics of triangular-notch thin-plate weirs. Studies of flow of water over weirs and dams.* Geological Survey Water-Supply Paper 1617-B. Washington, DC, USA: United States Department of the Interior. DOI: 10.3133/wsp1617B

Skertchly, M. L. (1988). *Manual de diseño de estructuras de aforo*. Jiutepec, México: Instituto Mexicano de Tecnología del Agua. Recovered from https://www.scribd.com/document/342624769/MANUAL-DISENO-ESTRUCTURAS-DE-AFORO-pdf

Sotelo, G. (1997). *Hidráulica general* (Vol. 1). México, DF, México: Editorial Limusa-Noriega. Recovered from https://www.academia.edu/38544755/Hidr%C3%A1ulica_General_Vol_1_Fundamentos_Gilberto_Sotelo_%C3%81vila

Spalart, P.R. and Allmaras, S.R., "A One-Equation Turbulence Model for Aerodynamics Flows", Boeing Commercial Airplane Group, Seattle, Washington, 1992.

Tian, Z., Wang, W., Bai, R., & Li, N. (2018). Effect of flaring gate piers on discharge coefficient for finite crest-length weirs. *Water*, 10(10), 1349. DOI: 10.3390/w10101349

USBR, United States Department of the Interior, Bureau of Reclamation. (1997). *Water measurement manual* (3rd ed.). Denver, USA: U.S. Government Printing Office. Recovered from https://www.usbr.gov/tsc/techreferences/mands/wmm/WMM_3rd_2001.pdf

Zahiri, A., Tang, X., & Azamathulla, H. Md. (2014). Mathematical modeling of flow discharge over compound sharp-crested weirs. *Journal of Hydro-Environment Research*, 8(3), 194-193. DOI: 10.1016/J.JHER.2014.01.001

Zuhair, A., & Zubaidy, R. (2013). Numerical simulation of two-phase flow. *International Journal of Structural and Civil Engineering Research*, 2(3). Recovered from http://www.ijscer.com/uploadfile/2015/0429/20150429074507182.pdf